IEEE Access
Multidisciplinary ⋮ Rapid Review ⋮ Open Access Journal

Received March 11, 2021, accepted April 3, 2021, date of publication April 20, 2021, date of current version May 3, 2021.

Digital Object Identifier 10.1109/ACCESS.2021.3074511

A Miniaturized MIMO Antenna With Triple Band-Notched Characteristics for UWB Applications

ZHIJIAN CHEN, WEISI ZHOU, AND JINGSONG HONG, (Member, IEEE)
School of Physical, Institute of Applied Physics, University of Electronic Science and Technology of China, Chengdu 611731, China

Corresponding author: Jingsong Hong (cemlab@uestc.edu.cn)

This work was supported in part by the National Natural Science Foundation of China under Grant 60872029 and Grant 61172115, in part by the High-Tech Research and Development Program of China under Grant 2008AA01Z206, in part by the Aeronautics Foundation of China under Grant 20100180003, and in part by the Fundamental Research Funds for the Central Universities under Grant ZYGX2009J037 and Grant 9140A07030513DZ02098.

ABSTRACT In this paper, a novel compact four-element ultra-wideband (UWB) multiple-input multiple-output (MIMO) antenna with triple band-notched characteristics is proposed. The proposed antenna is composed of four slot antenna elements with a common rhombic slot, each feeding by a microstrip-fed line to greatly reduce the overall size of the antenna. It has a compact size of 34 mm × 34 mm × 1.6 mm. The high isolation and polarization diversity are achieved by placing the four microstrip-fed lines perpendiculars to each other, while a parasitic strip is employed as a decoupling structure between adjacent microstrip-fed lines to further improve isolation. Moreover, the proposed antenna can achieve triple band-notched characteristics by embedding L-shaped and C-shaped slots on each radiator and loading electromagnetic band gap (EBG) structures next to micro-strip feeders respectively. As a result, the proposed antenna obtains three notched bands of 3.3-3.9 GHz, 5-6 GHz, and 7.4-8.5 GHz, which are in good agreement with the interference bands of WiMAX (3.3-3.7 GHz), WLAN (5.15-5.875 GHz) and X-band (7.3-8.5 GHz), respectively. The antenna prototype has been fabricated and measured. The results show that the antenna has an impedance bandwidth of 2.5-12 GHz (except for the three notched bands). Besides, the isolation among the elements, envelope correlation coefficient, radiation characteristics, efficiency, realized gain, and total active reflection coefficient are also investigated. The experimental results indicate that the proposed antenna can be a good candidate for UWB-MIMO wireless communication applications.

INDEX TERMS UWB-MIMO antenna, triple band-notched characteristics, electromagnetic band gap (EBG), compact size.

I. INTRODUCTION

With the development of wireless communication systems, high data rates and large channel capacity have been extensively studied by researchers in the past years. Ultrawideband (UWB) technology has drawn considerable attention for its high data rate, wide bandwidth, and low cost [1]. Due to the low transmission power, UWB technology is widely used in the field of short-range communications, radar, positioning, and tracking [2]–[5]. Diversity technology is utilized in the multiple-input multiple-output (MIMO) system to enable data transmission, thus effectively suppressing multipath fading and improving channel capacity [6]. In recent years, scholars have combined UWB technology with MIMO technology to develope UWB-MIMO technology [7]. UWB-MIMO technology makes full use of UWB and MIMO's advantages, effectively improving channel capacity and data rates and suppressing multipath fading. As an essential part of wireless communication systems, antennas are particularly important for UWB-MIMO communication systems. Therefore, UWB-MIMO antennas have attracted extensive attention and researches from scholars [8]–[11].

For the study of UWB-MIMO antennas, high isolation, miniaturization, and band-notched characteristics are three important research directions. There are various types of methods for miniaturization of antennas [12]–[17], such

The associate editor coordinating the review of this manuscript and approving it for publication was Yuan Yao.

as meandering [12], fractal technology [13], [14], loading [15], [16], and high dielectric constant substrate [17], etc. As the size of the antenna becomes more compact, the stronger mutual coupling between the antenna elements will result in a degradation of the antenna performance. The methods to reduce mutual coupling between antenna elements mainly include diversity technology [18]–[20], defected ground structure (DGS) [21]–[24], parasitic elements [25]–[28], neutralization line [29]–[32], electromagnetic bandgap structure (EBG) [33], [35], and decoupling networks [36]–[38], etc. To reject the interference with the wireless communication systems, a UWB-MIMO antenna with band-notched characteristics is required. Recently, different techniques to achieve band-notched characteristics are reported, such as etching slots [39]–[42], loading filter structures [43]–[46], etc. Meanwhile, some scholars have proposed the MIMO slot antenna to overcome the limitation of reducing antenna size. In [10], a UWB-MIMO slot antenna with a band-notched characteristic is presented; a T-shaped slot is etched on the ground to improve the impedance matching characteristic and enables the miniaturization of the antenna in [22]; In [40], a rhombic slot is introduced on the ground plane to reduce the dimension of the UWB-MIMO antenna, and a pair of L-shaped slit is etched to enable the notched band at 5.5 GHz; In [41], the wideband isolation is enhanced and a band-notched property is achieved by etching a 1/4 circular slot on the ground and a split-ring resonator (SRR) slot on each radiator respectively; In [58], a four-port MIMO antenna obtains compact size by etching four semicircular slots on the ground. However, it's quite difficult for UWB-MIMO antennas to simultaneously achieve small size, high isolation, and multiple band-notched characteristics. Therefore, getting a good performance for UWB-MIMO antennas under a compact size is a challenging task.

In this paper, a compact four-element UWB-MIMO slot antenna with triple band-notched characteristics is presented. The proposed four-port antenna has the same size of 34 mm × 34 mm × 1.6 mm as the antenna with only one slot radiation element. The antenna is composed of four slot antenna elements with a common rhombic slot, and they are symmetrically and orthogonally placed on the substrate. The overall size of the antenna can be greatly reduced by this design. A parasitic strip between adjacent microstrip-fed lines is used to reduce the mutual coupling among antenna elements. Furthermore, triple notched bands are achieved under a very small antenna size by etching two slots and loading EBG structures. The simulated and measured results indicate that the proposed UWB-MIMO antenna has a compact size, wide impedance bandwidth, low mutual coupling, good diversity performance, and triple band-notched characteristics.

II. ANTENNA DESIGN AND ANALYSIS

The geometry with parameters of the proposed UWB-MIMO antenna is illustrated in Fig. 1. The proposed antenna with an overall size of 34 mm × 34 mm × 1.6 mm is printed on an FR4 substrate with a relative dielectric constant of 4.4. It consists of four orthogonal microstrip-fed lines etched with two slits, four parasitic strips, four EBG structures, and a rhombic slot etched in the ground plane. The optimized design parameters are carried out by using electromagnetic simulation software HFSS. The optimal parameters are given in Tab. 1.

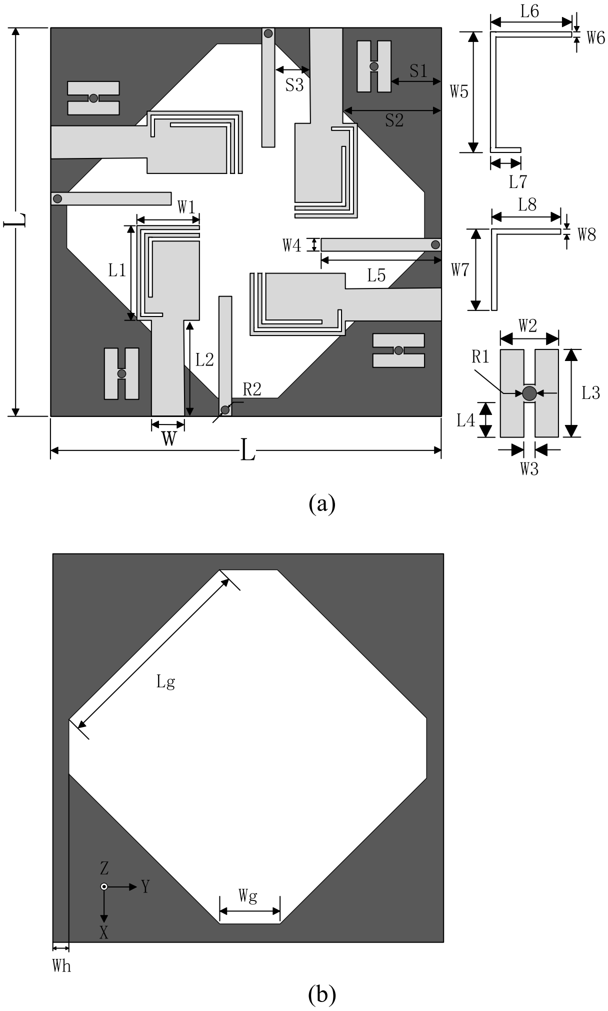

(a)

(b)

FIGURE 1. The geometry of the proposed UWB-MIMO antenna. (a) the top layer, (b) the bottom layer.

A. DESIGN OF UWB-MIMO ANTENNA ELEMENT

The design of the evolution of UWB-MIMO antenna elements is shown in Fig. 2. Initially, a wide-slot antenna with a rotated slot is designed in Fig. 2 (a). In [47], the impedance bandwidth of the antenna can be enhanced by etching a wide slot and then rotating the wide slot by 45°. Moreover, a wider impedance bandwidth can also be achieved by adopting an offset microstrip-line in [40]. That's because the antenna can generate multiple resonances to widen the impedance bandwidth. The simulation curve of the return loss S_{11} of antenna 1 is shown in Fig. 3. Antenna 1 generates two resonance points around 4 GHz and 5.5 GHz, which widen the impedance bandwidth of antenna 1. To make antenna 1 work

TABLE 1. Dimensions of optimized parameters for the proposed UWB-MIMO antenna.

Parameters	Dimensions (mm)	Parameters	Dimensions (mm)
L	34.0	W	3.0
L_1	8.0	W_1	5.0
L_2	7.0	W_2	3.0
L_3	4.6	W_3	0.4
L_4	0.8	W_4	1.0
L_5	11.0	W_5	7.2
L_6	4.6	W_6	0.4
L_7	1.8	W_7	4.8
L_8	3.9	W_8	0.4
R_1	0.3	R_2	0.3
S_1	4.5	S_2	8.5
S_3	2.5	L_g	12.5
W_g	2.0	W_h	2.0

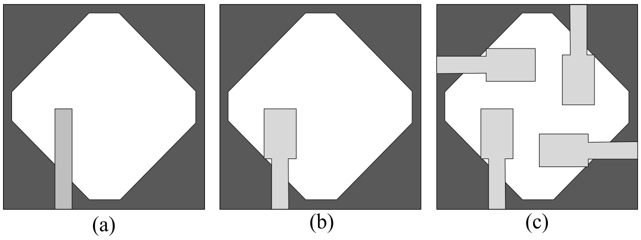
(a) (b) (c)

FIGURE 2. The design evolution of the UWB-MIMO element. (a) antenna 1, (b) antenna 2, (c) antenna 3.

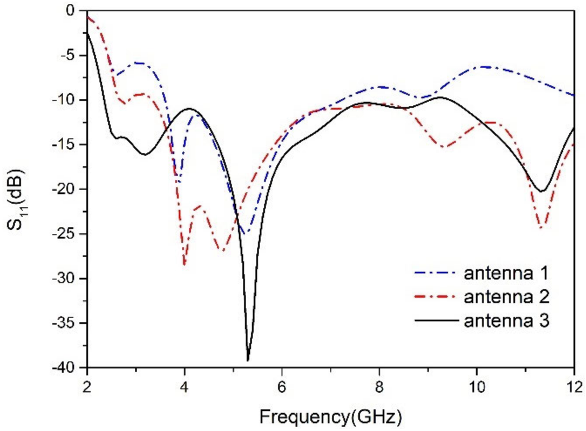

FIGURE 3. Simulated S_{11} of the UWB-MIMO antenna element with different configurations.

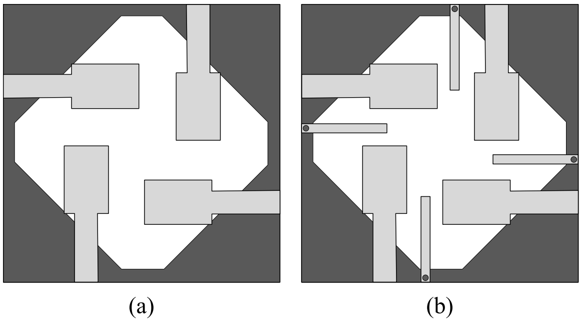
(a) (b)

FIGURE 4. The design evolution of the decoupling structure. (a) the antenna without the parasitic strips, (b) the antenna with the parasitic strips.

in the UWB band, a two-stage microstrip-line is used as an impedance transformer to improve the impedance matching at the low and high-frequency band (denoted as antenna 2). Finally, a 4-port UWB-MIMO antenna is formed by placing the four microstrip lines perpendiculars to each other, as shown in Fig. 2 (c). The size of the 4-port antenna is not increased and is the same as the size of antenna 2. Furthermore, in Fig. 3, the impedance bandwidth of the antenna is broadened at a lower frequency. This is mainly due to the addition of other microstrip-lines, which act as parasitic resonators to change the impedance matching and shift the resonance points.

B. DECOUPLING STRUCTURE DESIGN

Although the isolation can be improved by placing the four microstrip-lines perpendiculars to each other, the size of the antenna is so compact that the mutual coupling between the antenna elements is still strong. Then, to further reduce the mutual coupling, a parasitic strip is added between the adjacent microstrip-fed lines, as shown in Fig. 4. Usually, the parasitic strips are added on the ground as a reflection plate to suppress the mutual coupling among the antenna elements.

Since the proposed antenna in this paper is a slot antenna, adding parasitic strips on the ground will change the structure of the rhombic slot and greatly affect the impedance matching of the antenna. Therefore, the parasitic strips are placed on the top layer of the substrate, and they are connected to the ground by using vias. Fig. 5 illustrates the simulated S-parameters of the antenna with/without the parasitic strips. It's shown in Fig. 5 (a) that the addition of the decoupling structures will affect the impedance matching of the antenna in low and high-frequency bands. S-parameters S_{12} and S_{13} of the antenna are illustrated in Fig. 5 (b). After the parasitic strips are added, the isolation between the two adjacent antenna elements at 4-6 GHz is improved by about 5 dB and at 5-8 GHz, the isolation is increased by about 4 dB.

Fig. 6 shows the surface current distributions at 5 GHz when Port 1 is excited. Without the parasitic strips, the surface current is mainly concentrated on microstrip-lines and ground, and there is also a strong coupled current on adjacent microstrip-lines. By adding the parasitic strips, a larger surface current is induced along the parasitic strips, and the coupled current on adjacent microstrip-lines decreases substantially. Therefore, the mutual coupling between the antenna elements can be reduced by adopting the parasitic strips.

C. MULTIPLE NOTCHED BANDS DESIGN

To reject the interference with other wireless communication systems, the triple band-notched characteristic is achieved by etching two slits on each radiating patch and adding an EBG structure next to each microstrip-line.

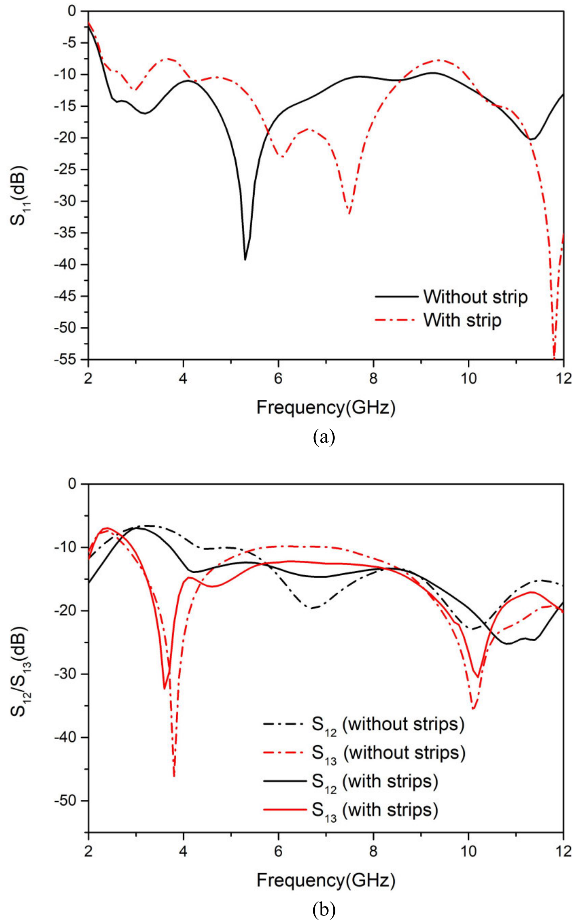

(a)

(b)

FIGURE 5. **Simulated S-parameters of the antenna with or without the decoupling structure. (a) S_{11}, (b) S_{12} /S_{13}.**

1) DESIGN OF ETCHING SLITS

Firstly, two notched bands of 3.3-3.9 GHz, 5-5.9 GHz are obtained by etching a C-shaped slit and an L-shaped slit on each radiator. The design evolution is shown in Fig. 7. The slits act as a quarter-wavelength resonator, the length of slits and resonant frequency can be calculated as

$$L_{S1} = L_6 + L_7 + W_5 \tag{1}$$

$$f_{S1} = \frac{c}{4L_{S1}\sqrt{\varepsilon_{reff}}} \tag{2}$$

where L_{S1} is the total length of the C-shaped slit, f_{s1} is the resonant frequency of the first notched band, $\varepsilon_{\text{reff}}$ is half of the dielectric constant of the FR4, due to the lack of ground, c is the speed of light. The length of L_{S1} is 13.6 mm and the resonant frequency f_{s1} is at 3.7 GHz by calculating. It can be seen from Fig. 8 that when the C-shaped slit is etched, the antenna generates a notched band around 3.6 GHz, which is similar to the calculation result.

The length of the L-shaped slit and the second resonant frequency can also be calculated as

$$L_{S2} = L_8 + W_7 \tag{3}$$

$$f_{S2} = \frac{c}{4L_{S2}\sqrt{\varepsilon_{reff}}} \tag{4}$$

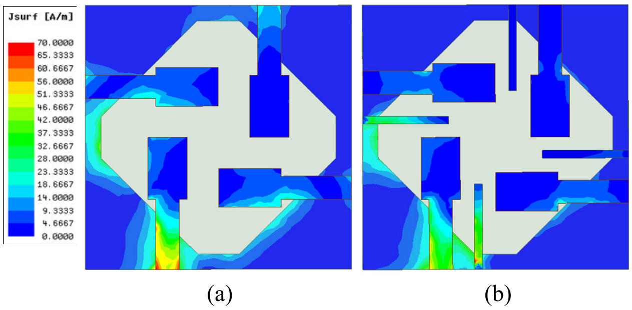

(a) (b)

FIGURE 6. **The surface current distribution of the antenna when Port 1 is excited at 5 GHz. (a) without decoupling structure, (b) with decoupling structure.**

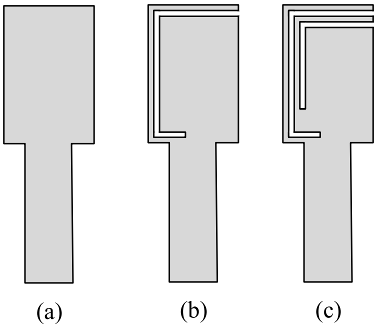

(a) (b) (c)

FIGURE 7. **The design evolution of multiple notched bands. (a) antenna A, (b) antenna B, (c) antenna C.**

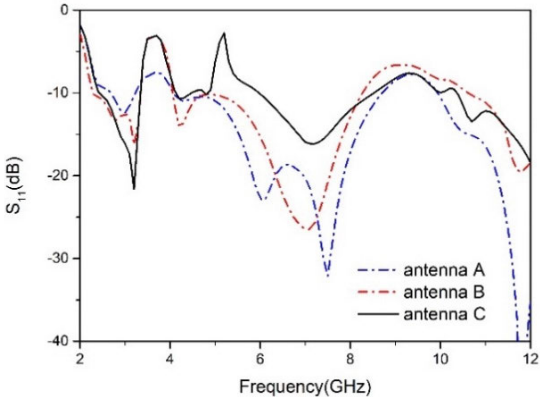

FIGURE 8. **Simulated S-parameters S_{11} of the antenna A/B/C.**

The length of L_{S2} is 8.8 mm and the second resonant frequency f_{s2} is at 5.7 GHz by calculating. It can be seen from Fig. 8 that the second resonant frequency is around 5.5 GHz, which is similar to the calculation result.

Fig. 9 shows the effect of the length of the two slits on the center frequency of the notched bands. Fig. 9 (a) shows when the total length L_{S1} of the C-shaped slit is reduced from 14.8 mm to 12.4 mm, the center frequency of the first notched band is increased from 3.5 GHz to 4.2 GHz. It can be seen from Fig. 9 (b) that when the total length L_{S2} of the L-shaped slit is reduced from 9.5 mm to 7.9 mm, the center frequency of the second notched band is increased from 5.4 GHz to 6.4 GHz. It is basically consistent with the result calculated by the formula.

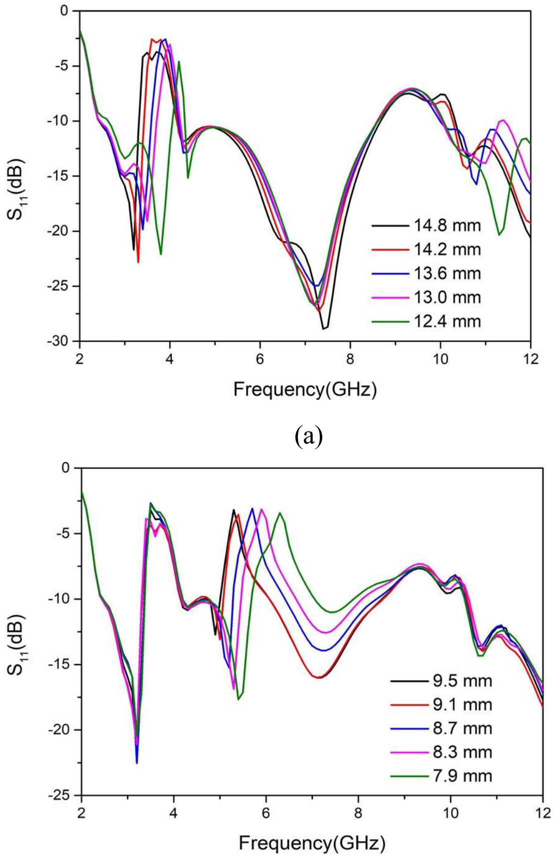

(a)

(b)

FIGURE 9. Simulated S-parameters S_{11} of the antenna with the different lengths of the two slits. (a) LS1, (b) LS2.

The principle of generating notched bands by etching slits is analyzed from the perspective of the vector current on the radiator surface. Fig. 10 (a) and (b) are the vector current distributions of the antenna when Port 1 is excited at 5.5 GHz and 3.6 GHz, respectively. When Port 1 is excited at 5.5 GHz, the surface current of the radiator is mainly concentrated on the L-shaped slit. It can be seen from the direction of the vector current that the current flows clockwise on the L-shaped slit, and the current flows counterclockwise on both sides of the L-shaped slit. Therefore, the radiation of the L-shaped slit is canceled by the radiation of both sides, and no effective radiation occurs around 5.5 GHz. When Port 1 is excited at 3.6 GHz, the surface current is mainly concentrated on the C-slit. Similarly, the radiation of the C-shaped slit is canceled by the radiation of both sides.

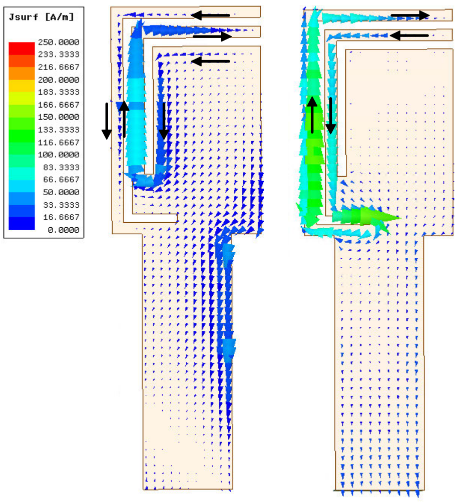

(a) (b)

FIGURE 10. Vector current distribution of the antenna. (a) at 5.5 GHz, (b) at 3.6 GHz.

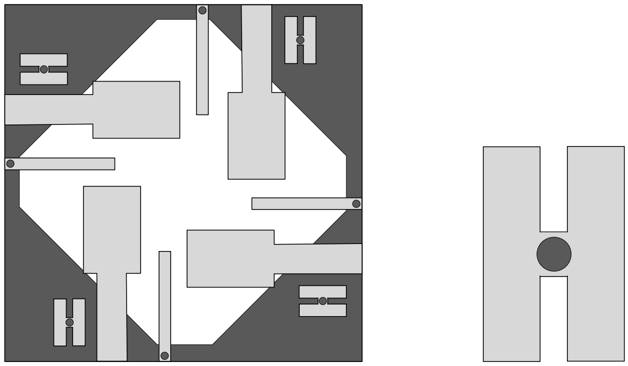

(a) (b)

FIGURE 11. The geometry of the antenna with EBG structures. (a) the antenna, (b) the EBG structure.

2) DESIGN OF EBG STRUCTURES

A mushroom-like EBG structure is introduced to achieve another band-notched characteristic. The electromagnetic band gap (EBG) structure has a band-gap characteristic, and it can be used to suppress the radiation of the antenna in the notched band. As shown in Fig. 11, the EBG structure consists of an H-shaped metallic patch and a metal via, which connects the patch into the ground. The notched band frequency and bandwidth of a simple mushroom-type EBG structure can be approximated by the expression in [43]. The simulated S_{11} of the antenna with or without the EBG structure is shown in Fig. 12. After adding the EBG structure, the antenna generates a notched band around 8 GHz.

Fig. 13 shows the surface current distributions of the antenna with or without the EBG structure at 8 GHz. When Port 1 is excited at 8 GHz, the surface current on the antenna is mainly concentrated on the EBG structure as shown in Fig. 13 (a). After adding the EBG structure, the radiant current is coupled to the EBG structure from the microstrip-line, so the antenna can't get sufficient radiation, and a notched band is formed around 8 GHz.

The equivalent circuit of the EBG structure is depicted in Fig. 14. The EBG structure and the microstrip-line can be equivalent to an LC resonant circuit. The capacitor C0 is due to the gap effect between the H-shaped patch and the microstrip-line, C1 results from the slit in the middle of the EBG, and L1 is due to the currents flowing through the via. They can be approximated by the expression in [43]. The

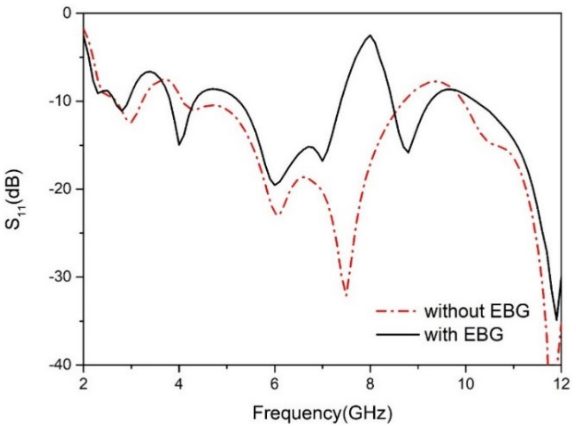

FIGURE 12. Simulated S-parameter S_{11} of the antenna with or without EBG structures.

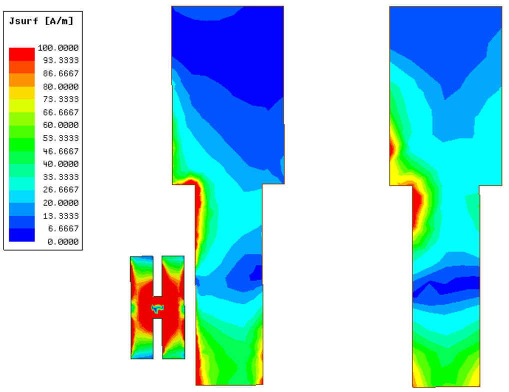

(a) (b)

FIGURE 13. The surface current distribution of the antenna at 8 GHz. (a) with the EBG structure, (b) without the EBG structure.

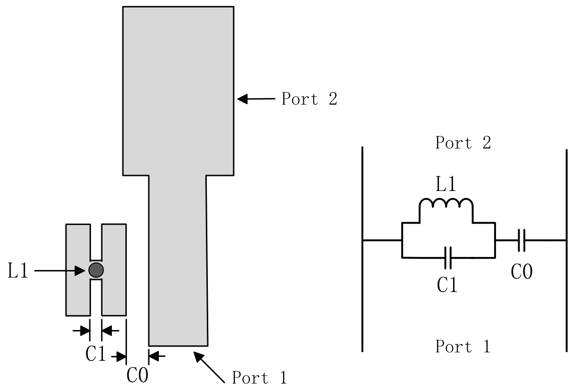

FIGURE 14. Equivalent circuit of the EBG structure and the microstrip-line.

impedance of the antenna with the EBG structure is given in Fig. 15, which shows the input impedance seen from Port 1. The real part of the impedance is very high at the notched band, and there is negligible current flows from Port 1 to Port 2. As can be seen in Fig. 14, the EBG structure is equivalent to a parallel LC resonator, and a high mismatch occurs at Port 1 due to high resistive impedance. Therefore, a notched band is achieved around 8 GHz by adding the EBG structure.

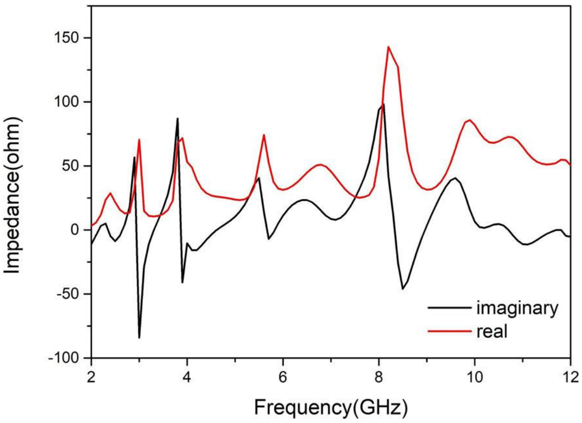

FIGURE 15. The input impedance of the antenna with the EBG structure.

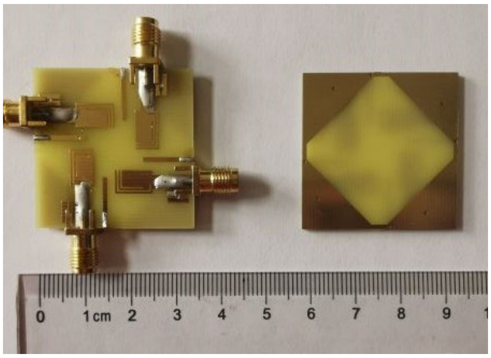

FIGURE 16. The physical diagram of the proposed antenna.

III. RESULTS AND DISCUSSIONS

The proposed 4-port UWB-MIMO antenna is fabricated and measured to verify the simulation results. S-parameters, the radiation patterns, radiation efficiency, and peak gain are the primary measurement parameters. When one of the antenna ports is excited during the measurement, the other ports are connected to a 50 Ω matching load. The S-Parameters of the antenna were measured by the vector network analyzer, and the radiation pattern and gain performance of the antenna was tested in a microwave anechoic chamber.

A. S-PARAMETERS

The antenna is fabricated on an FR4 dielectric substrate with a relative permittivity of 4.4 and a loss tangent angle of 0.025. The size of the 4-port antenna is 34 mm × 34 mm × 1.6 mm. Fig. 16 shows the physical diagram of the antenna, and Fig. 17 shows the S-parameters of the antenna. Fig. 17 (a) are the return loss curves of the four ports of the antenna. Due to the symmetry of the antenna, the S11 curves of the four ports are the same. It can be seen from Fig. 17 (a) that the S11 < -10 dB at 2.7-12 GHz. Meanwhile, three stopbands are generated at 3.4-4.1 GHz, 5-5.8 GHz, and 7.6-8.6 GHz. Due to the manufacture tolerance in the size of the EBG structure, the center frequency of the third stopband is shifted. Fig. 17 (b) shows the isolation curves between the four ports of the antenna. S12 is the isolation curve between adjacent antenna elements, and S13 is the isolation curve between

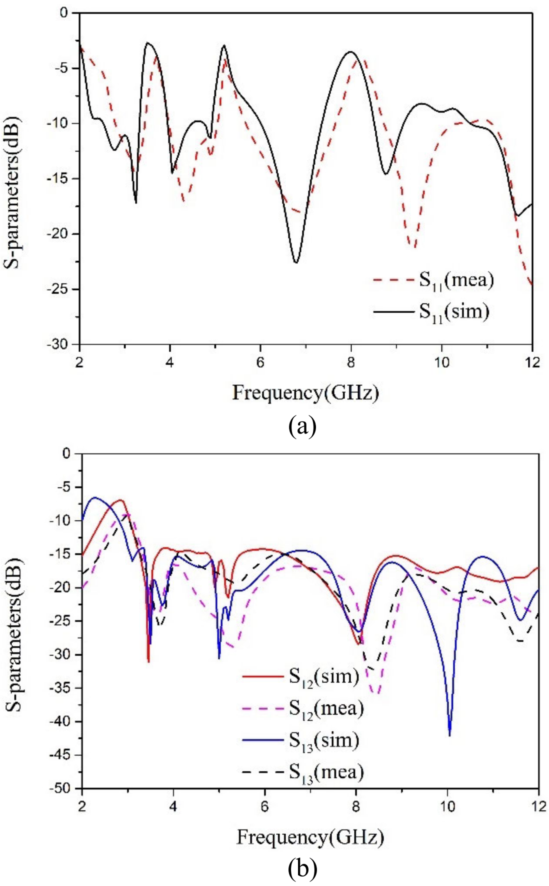

FIGURE 17. Simulated and measured results of S-parameters. (a) S11, S22, S33, and S44, (b) S12, S13, and S14.

diagonally opposite antenna elements. It can be seen from Fig. 17 (b) that the isolation degree of the antenna is higher than −15 dB in the whole UWB frequency band.

B. THE RADIATION PATTERNS

Fig. 18 shows the normalized two-dimensional radiation patterns of the UWB-MIMO antenna on the E-plane and H-plane when Port 1 is excited at 3 GHz, 5 GHz, 7 GHz, and 9 GHz, respectively. The solid lines are the simulation patterns of the antenna, and the dashed lines are the test patterns of the antenna. Due to the symmetry of the antenna structure, the radiation characteristics of Port 2-4 are the same as those of Port 1, which is not given here. As shown in Fig. 18, the radiation pattern of the antenna at low frequency is relatively stable. In the middle and high-frequency bands, the radiation patterns of the antenna change because of the notch structure. Fig. 18 shows that the test results of the antenna radiation patterns are consistent with the simulation results.

C. RADIATION EFFICIENCY AND PEAK GAIN

The peak gain and radiation efficiency of the antenna are shown in Fig. 19. The gain of the antenna is between 2.5-5.5 dBi in the entire UWB frequency band (excluding the notched band).

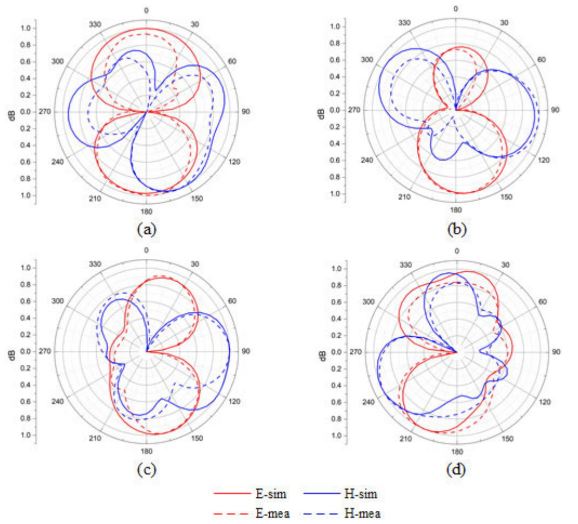

FIGURE 18. Simulated and measured radiation patterns of the proposed antenna. (a) at 3 GHz, (b) at 5 GHz, (c) at 7 GHz, (d) at 9 GHz.

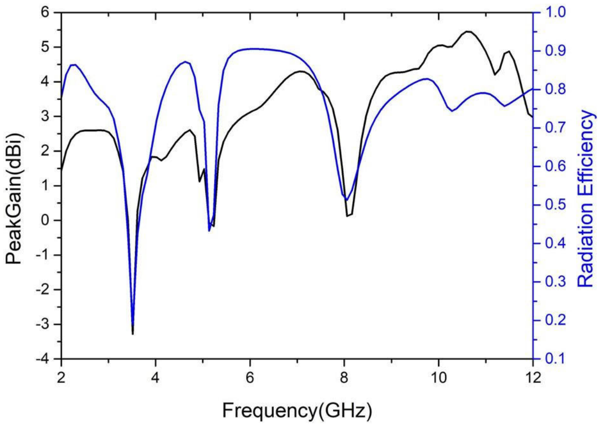

FIGURE 19. Radiation efficiency and peak gain of the proposed antenna.

In the notched band around 3.5 GHz, the gain is below 0 dBi, and the lowest value is −3.3 dBi. In the notched bands of 5.2 GHz and 8 GHz, the gain is the lowest around 0 dBi. This proves that the antenna has a good signal suppression effect in the notched band. The radiation efficiency of the antenna is between 75% and 90% in the entire UWB frequency band (excluding the notched band). In the triple notched frequency bands, the radiation efficiency of the antenna is below 50%. Moreover, the radiation efficiency of the antenna is only 15% at around 3.5 GHz.

D. DIVERSITY PERFORMANCE

The diversity performance of MIMO antennas is figured out by the envelope correlation coefficient(ECC) and the total active reflection coefficient(TARC). ECC is to measure the degree of correlation between adjacent antenna elements of MIMO antennas. The lower the ECC, the lower the correlation between the antenna elements, which is usually required to be lower than 0.5. ECC can be calculated from the radiation field function of each antenna element, for a two-element

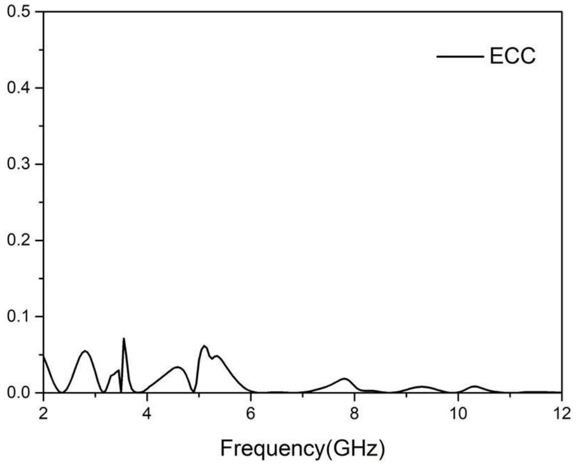

FIGURE 20. Envelope correlation coefficient of the proposed antenna.

MIMO antenna, ECC is defined as

$$\rho_e = \frac{\left| \iint_{4\pi} \left[F_1(\theta,\varphi) \cdot F_2(\theta,\varphi) \right] d\Omega \right|^2}{\iint_{4\pi} \left| F_1(\theta,\varphi) \right|^2 d\Omega \cdot \iint_{4\pi} \left| F_2(\theta,\varphi) \right|^2 d\Omega} \tag{5}$$

When the antenna radiation efficiency is high, the ECC of the MIMO antenna can be approximately calculated by the S-parameters, the formula is as follows [55]:

$$ECC = \frac{\left| S_{ii}^{*} S_{ij} + S_{ji}^{*} S_{jj} \right|^2}{\left| \left(1 - |S_{ii}|^2 - |S_{ji}|^2\right) \cdot \left(1 - |S_{jj}|^2 - |S_{ij}|^2\right) \right|} \tag{6}$$

Fig. 20 shows the ECC diagram of the antenna. It can be seen from Fig. 20 that the ECC of the antenna is less than 0.05 in the UWB frequency band, indicating that the correlation between the antenna elements is very small, and the antenna can work well in the MIMO system. The notched frequency band ECC > 0.05 proves that the antenna performance is reduced in the notched frequency band.

TARC is defined as the ratio of the square root of total reflected power divided by the square root of total incident power [61]–[64]. To accurately characterize the return loss of the whole MIMO antenna system and the effect of change in phase of I/p signal on the BW of the MIMO antenna, it typically takes less than 0 dB. The TARC of the 4-port MIMO antenna can be calculated from the S-parameters using the formula (7), as shown at the bottom of the page, [63]:

Fig. 21 shows the TARC plot of the antenna. By selecting ten sets of random phases$(\theta, \theta', \theta'')$, we obtain a TARC curve family composed of ten curves. It can be seen from Fig. 21 that all the TARC curves are less than 0 dB in the UWB frequency band, and all the elements of the curve family show strong convergence, which indicates that the proposed antenna is not sensible to phase changes. It shows that the UWB-MIMO antenna has a good performance in the MIMO system.

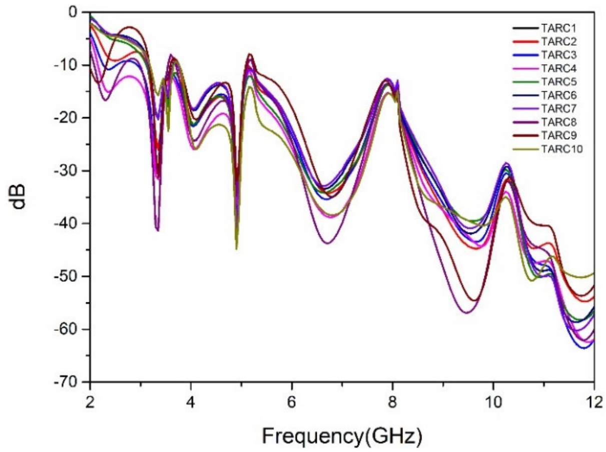

FIGURE 21. Total active reflection coefficient of the proposed antenna.

TABLE 2. Comparisons between the proposed antenna and other works.

Ref.	Dimension (mm^3)	Isolation (dB)	ECC	Number of notch bands	Gain (dBi)
[25]	50×30×1.6	>20	<0.04	0	0.1~4.0
[41]	48×48×0.8	>15	<0.005	1	1.5~6.5
[48]	50×40×1.6	>17	<0.025	1	2.0~5.7
[49]	40×40×0.8	>20	<0.002	0	1.3~4.0
[50]	38×38×0.8	>15	<0.2	0	0.5~5.0
[51]	45×45×1.6	>17	<0.005	1	1.5~4.5
[52]	50×40×1.5	>17	<0.01	1	2.5~6.0
[53]	44×44×1.6	>15.5	<0.04	1	2.4~4.0
[54]	39×39×1.6	>22	<0.02	3	1.4~4.6
[55]	64×45×1.6	>15	<0.02	3	0~6.0
[56]	48×48×0.8	>20	NA	0	2.0~4.5
[57]	50×40×1.6	>15	<0.01	0	2.1~8.9
[58]	40×40×1.6	>17	<0.03	0	1.0~5.0
[59]	50×35×1.0	>25	<0.004	0	4.0~6.0
[60]	55×55×1.6	>20	<0.13	0	1.5~4.2
Prop.	34×34×1.6	>15	<0.05	3	2.5~5.5

E. COMPARISON OF VARIOUS UWB-MIMO ANTENNAS

A comparison between the proposed antenna and other antennas given in references is provided in Tab. 2. All the compared

$$TARC = \frac{\sqrt{\begin{array}{l} \left|\left(s_{11} + s_{12}e^{j\theta} + s_{13}e^{j\theta'} + s_{14}e^{j\theta''}\right)\right|^2 + \left|\left(s_{21} + s_{22}e^{j\theta} + s_{23}e^{j\theta'} + s_{24}e^{j\theta''}\right)\right|^2 \\ + \left|\left(s_{31} + s_{32}e^{j\theta} + s_{33}e^{j\theta'} + s_{34}e^{j\theta''}\right)\right|^2 + \left|\left(s_{41} + s_{42}e^{j\theta} + s_{43}e^{j\theta'} + s_{44}e^{j\theta''}\right)\right|^2 \end{array}}}{2} \tag{7}$$

UWB-MIMO antennas have small sizes. However, it is quite difficult to achieve multiple notches and high isolation under a compact antenna size. The proposed 4-port UWB-MIMO antenna not only has a more compact size than other antennas but also achieves triple band-notched characteristics, better isolation, and higher gain.

IV. CONCLUSION

In this paper, a miniaturized UWB-MIMO antenna with triple band-notched characteristics in size of $34 \times 34 \times 1.6$ mm^3 has been designed successfully. The antenna is miniaturized by sharing rhombic slot radiation with four microstrip feeders, and the notched characteristics of the three frequency bands are realized by opening C-slot, L-slot, and adding an H-shaped EBG structure. Measured outcomes show that the designed antenna exhibits $S11 < -10$ dB, high isolation better than 40 dB, peak gain varies 2.5 dBi to 5.5 dBi, radiation efficiency varies 75% to 90%, $ECC < 0.05$ and $TARC < -40$ dB over the UWB band except for three notched bands at 3.3-3.9 GHz, 5-6 GHz, and 7.4-8.5 GHz. Besides, the antenna elements of the proposed antenna are placed according to an orthogonal rotation scheme, which involves a simple and straightforward manufacturing process. All the measured, simulated, and calculated results indicate the proposed 4-port MIMO antenna is a good candidate for UWB applications.

REFERENCES

[1] M. G. N. Alsath and M. Kanagasabai, "Compact UWB monopole antenna for automotive communications," *IEEE Trans. Antennas Propag.*, vol. 63, no. 9, pp. 4204–4208, Sep. 2015.

[2] E. M. Staderini, "UWB radars in medicine," *IEEE Aerosp. Electron. Syst. Mag.*, vol. 17, no. 1, pp. 13–18, Jan. 2002.

[3] J. Zhang, P. V. Orlik, Z. Sahinoglu, A. F. Molisch, and P. Kinney, "UWB systems for wireless sensor networks," *Proc. IEEE*, vol. 97, no. 2, pp. 313–331, Feb. 2009.

[4] B. Sobhani, E. Paolini, A. Giorgetti, M. Mazzotti, and M. Chiani, "Target tracking for UWB multistatic radar sensor networks," *IEEE J. Sel. Topics Signal Process.*, vol. 8, no. 1, pp. 125–136, Feb. 2014.

[5] R. Kshetrimayum, "An introduction to UWB communication systems," *IEEE Potentials*, vol. 28, no. 2, pp. 9–13, Mar./Apr. 2009.

[6] C. King, "Fundamentals of wireless communications," presented at the 67th Annu. Conf. Protective Relay Eng., College Station, TX, USA, 2014.

[7] M. Weisenhorn and W. Hirt, "Performance of binary antipodal signaling over indoor UWB MIMO channel," presented at the IEEE Int. Conf. Commun., Anchorage, AK, USA, 2003.

[8] M. Bilal, R. Saleem, H. H. Abbasi, M. F. Shafique, and A. K. Brown, "An FSS-based nonplanar quad-element UWB-MIMO antenna system," *IEEE Antennas Wireless Propag. Lett.*, vol. 16, pp. 987–990, 2017.

[9] X. Zhao, S. P. Yeo, and L. C. Ong, "Planar UWB MIMO antenna with pattern diversity and isolation improvement for mobile platform based on the theory of characteristic modes," *IEEE Trans. Antennas Propag.*, vol. 66, no. 1, pp. 420–425, Jan. 2018.

[10] G. Irene and A. Rajesh, "A dual-polarized UWB–MIMO antenna with IEEE 802.11ac band-notched characteristics using split-ring resonator," *J. Comput. Electron.*, vol. 17, no. 3, pp. 1090–1098, Sep. 2018.

[11] S. Rajkumar, K. T. Selvan, and P. H. Rao, "Compact 4 element sierpinski knopp fractal UWB MIMO antenna with dual band notch," *Microw. Opt. Technol. Lett.*, vol. 60, no. 4, pp. 1023–1030, Apr. 2018.

[12] S. Das, P. Chowdhury, A. Biswas, P. P. Sarkar, and S. K. Chowdhury, "Analysis of a miniaturized multiresonant wideband slotted microstrip antenna with modified ground plane," *IEEE Antennas Wireless Propag. Lett.*, vol. 14, pp. 60–63, 2015.

[13] J. Pourahmadazar, C. Ghobadi, and J. Nourinia, "Novel modified pythagorean tree fractal monopole antennas for UWB applications," *IEEE Antennas Wireless Propag. Lett.*, vol. 10, pp. 484–487, 2011.

[14] A. Azari, A. Ismail, A. Sali, and F. Hashim, "A new super wideband fractal monopole-dielectric resonator antenna," *IEEE Antennas Wireless Propag. Lett.*, vol. 12, pp. 1014–1016, 2013.

[15] M. Yang, Z. N. Chen, P. Y. Lau, X. Qing, and X. Yin, "Miniaturized patch antenna with grounded strips," *IEEE Trans. Antennas Propag.*, vol. 63, no. 2, pp. 843–848, Feb. 2015.

[16] H. Malekpoor and S. Jam, "Enhanced bandwidth of shorted patch antennas using folded-patch techniques," *IEEE Antennas Wireless Propag. Lett.*, vol. 12, pp. 198–201, 2013.

[17] S. Chen, G. Liu, X. Chen, T. Lin, X. Liu, and Z. Duan, "Compact dual-band GPS microstrip antenna using multilayer LTCC substrate," *IEEE Antennas Wireless Propag. Lett.*, vol. 9, pp. 421–423, 2010.

[18] L. Liu, S. W. Cheung, and T. I. Yuk, "Compact MIMO antenna for portable devices in UWB applications," *IEEE Trans. Antennas Propag.*, vol. 61, no. 8, pp. 4257–4264, Aug. 2013.

[19] J. Zhu, S. Li, B. Feng, L. Deng, and S. Yin, "Compact dual-polarized UWB quasi-self-complementary MIMO/diversity antenna with band-rejection capability," *IEEE Antennas Wireless Propag. Lett.*, vol. 15, pp. 905–908, 2016.

[20] Y. Sharma, D. Sarkar, K. Saurav, and K. V. Srivastava, "Three-element MIMO antenna system with pattern and polarization diversity for WLAN applications," *IEEE Antennas Wireless Propag. Lett.*, vol. 16, pp. 1163–1166, 2017.

[21] J.-F. Li, Q.-X. Chu, and T.-G. Huang, "A compact wideband MIMO antenna with two novel bent slits," *IEEE Trans. Antennas Propag.*, vol. 60, no. 2, pp. 482–489, Feb. 2012.

[22] C.-M. Luo, J.-S. Hong, and L.-L. Zhong, "Isolation enhancement of a very compact UWB-MIMO slot antenna with two defected ground structures," *IEEE Antennas Wireless Propag. Lett.*, vol. 14, pp. 1766–1769, 2015.

[23] R. Anitha, V. P. Sarin, P. Mohanan, and K. Vasudevan, "Enhanced isolation with defected ground structure in MIMO antenna," *Electron. Lett.*, vol. 50, no. 24, pp. 1784–1786, Nov. 2014.

[24] V. Satam and S. Nema, "Two element compact UWB diversity antenna with combination of DGS and parasitic elements," *Wireless Pers. Commun.*, vol. 98, no. 3, pp. 2901–2911, Feb. 2018.

[25] A. Iqbal, O. A. Saraereh, A. W. Ahmad, and S. Bashir, "Mutual coupling reduction using F-shaped stubs in UWB-MIMO antenna," *IEEE Access*, vol. 6, pp. 2755–2759, 2018.

[26] M. A. Ul Haq and S. Koziel, "Ground plane alterations for design of high-isolation compact wideband MIMO antenna," *IEEE Access*, vol. 6, pp. 48978–48983, 2018.

[27] A. I. Najam, Y. Duroc, and S. Tedjni, "UWB-MIMO antenna with novel stub structure," *Prog. Electromagn. Res. C*, vol. 19, pp. 245–257, Feb. 2011.

[28] M. S. Khan, A.-D. Capobianco, S. M. Asif, D. E. Anagnostou, R. M. Shubair, and B. D. Braaten, "A compact CSRR-enabled UWB diversity antenna," *IEEE Antennas Wireless Propag. Lett.*, vol. 16, pp. 808–812, 2017.

[29] S. Zhang and G. F. Pedersen, "Mutual coupling reduction for UWB MIMO antennas with a wideband neutralization line," *IEEE Antennas Wireless Propag. Lett.*, vol. 15, pp. 166–169, 2016.

[30] S.-W. Su, C.-T. Lee, and F.-S. Chang, "Printed MIMO-antenna system using neutralization-line technique for wireless USB-dongle applications," *IEEE Trans. Antennas Propag.*, vol. 60, no. 2, pp. 456–463, Feb. 2012.

[31] S.-W. Su and C.-T. Lee, "Printed two monopole-antenna system with a decoupling neutralization line for 2.4-GHz MIMO applications," *Microw. Opt. Technol. Lett.*, vol. 53, no. 9, pp. 2037–2043, Sep. 2011.

[32] W. H. Shin, S. Kibria, and M. T. Islam, "Hexa band MIMO antenna with neutralization line for LTE mobile device application," *Microw. Opt. Technol. Lett.*, vol. 58, no. 5, pp. 1198–1204, May 2016.

[33] S. Ghosh, T.-N. Tran, and T. Le-Ngoc, "Dual-layer EBG-based miniaturized multi-element antenna for MIMO systems," *IEEE Trans. Antennas Propag.*, vol. 62, no. 8, pp. 3985–3997, Aug. 2014.

[34] X. Yang, Y. Liu, Y.-X. Xu, and S.-X. Gong, "Isolation enhancement in patch antenna array with fractal UC-EBG structure and cross slot," *IEEE Antennas Wireless Propag. Lett.*, vol. 16, pp. 2175–2178, 2017.

[35] S. R. Thummaluru, R. Kumar, and R. K. Chaudhary, "Isolation enhancement and radar cross section reduction of MIMO antenna with frequency selective surface," *IEEE Trans. Antennas Propag.*, vol. 66, no. 3, pp. 1595–1600, Mar. 2018.

[36] B. C. Pan and T. J. Cui, "Broadband decoupling network for dual-band microstrip patch antennas," *IEEE Trans. Antennas Propag.*, vol. 65, no. 10, pp. 5595–5598, Oct. 2017.

[37] L. Zhao and K.-L. Wu, "A dual-band coupled resonator decoupling network for two coupled antennas," *IEEE Trans. Antennas Propag.*, vol. 63, no. 7, pp. 2843–2850, Jul. 2015.

[38] J. Baek and J. Choi, "The design of a LTE/MIMO antenna with high isolation using a decoupling network," *Microw. Opt. Technol. Lett.*, vol. 56, no. 9, pp. 2187–2191, Sep. 2014.

[39] R. Chandel, A. K. Gautam, and K. Rambabu, "Tapered fed compact UWB MIMO-diversity antenna with dual band-notched characteristics," *IEEE Trans. Antennas Propag.*, vol. 66, no. 4, pp. 1677–1684, Apr. 2018.

[40] L. Kang, H. Li, X. Wang, and X. Shi, "Compact offset microstrip-fed MIMO antenna for band-notched UWB applications," *IEEE Antennas Wireless Propag. Lett.*, vol. 14, pp. 1754–1757, 2015.

[41] P. Gao, S. He, X. Wei, Z. Xu, N. Wang, and Y. Zheng, "Compact printed UWB diversity slot antenna with 5.5-GHz band-notched characteristics," *IEEE Antennas Wireless Propag. Lett.*, vol. 13, pp. 376–379, 2014.

[42] A. K. Gautam, S. Yadav, and K. Rambabu, "Design of ultra-compact UWB antenna with band-notched characteristics for MIMO applications," *IET Microw., Antennas Propag.*, vol. 12, no. 12, pp. 1895–1900, Oct. 2018.

[43] M. Yazdi and N. Komjani, "Design of a band-notched UWB monopole antenna by means of an EBG structure," *IEEE Antennas Wireless Propag. Lett.*, vol. 10, pp. 170–173, 2011.

[44] L. Liu, S. W. Cheung, and T. I. Yuk, "Compact MIMO antenna for portable UWB applications with band-notched characteristic," *IEEE Trans. Antennas Propag.*, vol. 63, no. 5, pp. 1917–1924, May 2015.

[45] G. S. Reddy, A. Kamma, S. K. Mishra, and J. Mukherjee, "Compact Bluetooth/UWB dual-band planar antenna with quadruple band-notch characteristics," *IEEE Antennas Wireless Propag. Lett.*, vol. 13, pp. 872–875, 2014.

[46] R. Chandel and A. K. Gautam, "Compact MIMO/diversity slot antenna for UWB applications with band-notched characteristic," *Electron. Lett.*, vol. 52, no. 5, pp. 336–338, Mar. 2016.

[47] J.-Y. Jan and Jia, "Bandwidth enhancement of a printed wide-slot antenna with a rotated slot," *IEEE Trans. Antennas Propag.*, vol. 53, no. 6, pp. 2111–2114, Jun. 2005.

[48] S. M. Khan, A. Iftikhar, S. M. Asif, A.-D. Capobianco, and B. D. Braaten, "A compact four elements UWB MIMO antenna with on-demand WLAN rejection," *Microw. Opt. Technol. Lett.*, vol. 58, no. 2, pp. 270–276, Feb. 2016.

[49] W. A. E. Ali and A. A. Ibrahim, "A compact double-sided MIMO antenna with an improved isolation for UWB applications," *AEU-Int. J. Electron. Commun.*, vol. 82, pp. 7–13, Dec. 2017.

[50] D. Sipal, M. P. Abegaonkar, and S. K. Koul, "Easily extendable compact planar UWB MIMO antenna array," *IEEE Antennas Wireless Propag. Lett.*, vol. 16, pp. 2328–2331, 2017.

[51] S. Tripathi, A. Mohan, and S. Yadav, "A compact koch fractal UWB MIMO antenna with WLAN band-rejection," *IEEE Antennas Wireless Propag. Lett.*, vol. 14, pp. 1565–1568, 2015.

[52] M. S. Khan, A. D. Capobianco, S. Asif, A. Iftikhar, B. Ijaz, and B. D. Braaten, "Compact 4×4 UWB-MIMO antenna with WLAN band rejected operation," *Electron. Lett.*, vol. 51, no. 14, pp. 1048–1050, Jul. 2015.

[53] Y.-Y. Liu and Z.-H. Tu, "Compact differential band-notched stepped-slot UWB-MIMO antenna with common-mode suppression," *IEEE Antennas Wireless Propag. Lett.*, vol. 16, pp. 593–596, 2017.

[54] Z. Tang, X. Wu, J. Zhan, S. Hu, Z. Xi, and Y. Liu, "Compact UWB-MIMO antenna with high isolation and triple band-notched characteristics," *IEEE Access*, vol. 7, pp. 19856–19865, 2019.

[55] N. Jaglan, S. D. Gupta, E. Thakur, D. Kumar, B. K. Kanaujia, and S. Srivastava, "Triple band notched mushroom and uniplanar EBG structures based UWB MIMO/diversity antenna with enhanced wide band isolation," *AEU-Int. J. Electron. Commun.*, vol. 90, pp. 36–44, Jun. 2018.

[56] C.-X. Mao and Q.-X. Chu, "Compact coradiator UWB-MIMO antenna with dual polarization," *IEEE Trans. Antennas Propag.*, vol. 62, no. 9, pp. 4474–4480, Sep. 2014.

[57] G.-S. Lin, C.-H. Sung, J.-L. Chen, L.-S. Chen, and M.-P. Houng, "Isolation improvement in UWB MIMO antenna system using carbon black film," *IEEE Antennas Wireless Propag. Lett.*, vol. 16, pp. 222–225, 2017.

[58] A. A. R. Saad and H. A. Mohamed, "Conceptual design of a compact four-element UWB MIMO slot antenna array," *IET Microw., Antennas Propag.*, vol. 13, no. 2, pp. 208–215, Feb. 2019.

[59] L. Wang, Z. Du, H. Yang, R. Ma, Y. Zhao, X. Cui, and X. Xi, "Compact UWB MIMO antenna with high isolation using fence-type decoupling structure," *IEEE Antennas Wireless Propag. Lett.*, vol. 18, no. 8, pp. 1641–1645, Aug. 2019.

[60] A. Toktas and A. Akdagli, "Compact multiple-input multiple-output antenna with low correlation for ultra-wide-band applications," *IET Microw., Antennas Propag.*, vol. 9, no. 8, pp. 822–829, Jun. 2015.

[61] M. Manteghi and Y. Rahmat-Samii, "Multiport characteristics of a wide-band cavity backed annular patch antenna for multipolarization operations," *IEEE Trans. Antennas Propag.*, vol. 53, no. 1, pp. 466–474, Jan. 2005.

[62] S. H. Chae, S.-K. Oh, and S.-O. Park, "Analysis of mutual coupling, correlations, and TARC in WiBro MIMO array antenna," *IEEE Antennas Wireless Propag. Lett.*, vol. 6, pp. 122–125, 2007.

[63] S. H. Chae, W. I. Kawk, S. Park, and K. Lee, "Analysis of mutual coupling in MIMO antenna array by TARC calculation," presented at the Asia–Pacific Microw. Conf., Yokohama, Japan, 2006.

[64] D. W. Browne, M. Manteghi, M. P. Fitz, and Y. Rahmat-Samii, "Experiments with compact antenna arrays for MIMO radio communications," *IEEE Trans. Antennas Propag.*, vol. 54, no. 11, pp. 3239–3250, Nov. 2006.

ZHIJIAN CHEN was born in Chengdu, Sichuan, China, in 1994. He received the B.S. degree in electronic information engineering from the Chengdu University of Information Technology, in 2017, and the M.S. degree in electronics and communications engineering from the University of Electronic Science and Technology of China (UESTC), in 2020. His research interests include UWB-MIMO antenna and MIMO systems.

WEISI ZHOU was born in Anqing, Anhui, China, in 1995. He received the B.S. degree in electronic information engineering from the Shandong University of Technology, in 2018. He is currently pursuing the M.S. degree in electronics and communications engineering with the University of Electronic Science and Technology of China (UESTC). His research interests include MIMO antenna decoupling and antenna design.

JINGSONG HONG (Member, IEEE) received the B.Sc. degree in electromagnetics from Lanzhou University, China, in 1991, and the M.Sc. and Ph.D. degrees in electrical engineering from the University of Electronic Science and Technology of China (UESTC), in 2000 and 2005, respectively.

From 1991 to 1993, he was a Circuit Designer with Jingjiang Radar Factory, Chengdu, China. From 1993 to 1997, he was a Testing Engineer with SAE Magnetics (HK) Ltd., Guangdong, China. From 1999 to 2002, he was a Research Assistant with the City University of Hong Kong. He is currently a Professor with UESTC. He has authored more than 50 research articles. His research interests include the use of numerical techniques in electromagnetics and the use of microwave methods for materials characterization and processing.

Dr. Hong is also responsible for the National 863 Project, the Natural Science Foundation Project, the Military 863 Innovation Fund, the Aviation Science Foundation, and other scientific research projects. He is also a deputy editor or a reviewer of many American magazines and a reviewer of many domestic magazines.

• • •